Scientific Papers. Series E. Land Reclamation, Earth Observation & Surveying, Environmental Engineering. Vol. XIV, 2025
Print ISSN 2285-6064, CD-ROM ISSN 2285-6072, Online ISSN 2393-5138, ISSN-L 2285-6064

INTEGRATING UAS, LiDAR, AND GROUND-BASED SURVEYING FOR PRECISE DEMOLITION VOLUME ASSESSMENT: A CASE STUDY OF THE DOLJ CHIM INDUSTRIAL COMPLEX

George CRISTIAN, Sorin HERBAN, Carmen GRECEA, Clara-Beatrice VÎLCEANU, Andreea Diana CLEPE

Politehnica University of Timișoara, 2 Traian Lalescu Street, 300223, Timișoara, Romania

Corresponding author email: beatrice.vilceanu@upt.ro

Abstract

This study presents a case analysis of an integrated surveying and mapping initiative conducted at the Dolj Chim industrial complex in Romania, with the primary objective of determining material volumes expected from impending demolition activities. Employing a multi-faceted approach, the research combined data acquisition using a handheld LiDAR system for the interior and data acquired through a UAS equipped with high-resolution imaging sensors for the exterior. These complementary datasets were georeferenced using ground control points collected via Global Positioning System (GPS) receivers and Total Station measurements, ensuring a consistently accurate and spatially coherent representation of the site. This integrated approach streamlines data management and enhances the utility of subsequent analyses. The results emphasize the significance of selecting and integrating appropriate surveying technologies tailored to the complexities of industrial environments. By leveraging the strengths of various methods, high-density interior scanning and external imaging, reinforced by reliable ground-based control, the study achieves an enriched and precise dataset conducive to informed decision-making in demolition planning. Beyond its immediate relevance, this approach demonstrates broader applicability in complex geospatial contexts, illuminating best practices for harmonizing sensor technologies and conventional surveying techniques. Consequently, the research contributes insights into optimizing data quality, operational efficiency, and overall methodological rigor in contemporary geospatial applications.

Key words*: LiDAR, photogrammetry, industrial survey, demolition planning, 3D modelling, Romania.*

INTRODUCTION

This paper explores the crucial role that surveying and mapping plays in various engineering and geospatial applications and the implementation of integrated surveying techniques in the context of the Dolj Chim industrial complex demolition project.

The main objective of the study is to quantify the volumes of various construction materials (e.g. concrete, iron, wood, glass etc.) that will result from the demolition process, by harnessing the synergetic potential LiDAR scanning for interior spaces and UAS based photogrammetry for the roof of the buildings and surrounding area. In the case of industrial demolition, precise 3D modelling is essential to ensure cost-effective waste management while complying with environmental and work safety regulations, as underscored by (Nikmehr et al., 2021).

While traditional surveying methods can be time-consuming and challenging in degraded industrial environments (Zhan et al. 2020), this study aims to demonstrate the efficiency of integrating LiDAR, UAS photogrammetry and ground-based control points to achieve an accurate and comprehensive 3D model for demolition planning.

This project presented challenges that are common in old industrial complexes throughout Romania due to their advanced state of degradation, including water damage, overgrown vegetation and hazardous conditions such as shattered glass and unstable structures (Matsimbe et al., 2022).

The aim of this study is to highlight how modern surveying technologies complement traditional methods, leading to improved data acquisition and processing efficiency in complex industrial areas, offering a template for best practices in the field.

MATERIALS AND METHODS

In modern surveying, SLAM and UAS both enable spatial data acquisition. SLAM's real-time 3D mapping suits complex indoor environments, ensuring mobility. Meanwhile,

UAS excels at broad aerial surveys. The optimal choice depends on specific project needs, environment, and data requirements. A GeoSLAM Zeb Horizon RT LiDAR scanner (Figure 1) was used to scan the interior of the buildings and the ground level of the entire complex. The technical specifications of the GeoSLAM Zeb Horizon, which was used in the data acquisition process, are presented in Table 1.

Figure 1. GeoSLAM Zeb Horizon RT

Table 1. GeoSLAM Zeb Horizon technical specifications

Scanner	
Type	VLP-16
Acquisition	300.000 pts/sec
Channels	16
Range	100 m
Class	Class 1 eye safe laser
Wavelength	903 nm
Angular resolution	2°
Angular resolution	0.1-0.4°
Weight	1.3 kg
Raw data file size	100-200 MB a minute
Rotation	10 Hz
Datalogger	
Battery	PAG L90 SLIM, 90 Wh, 14.8V, 6.1 Ah
Operational time	3.5 hours
Storage	120 GB
Operational temp	0 – 50°
Weight	2.4 kg
System	
Protection Class	IP54
Processing	Post
Accuracy	1-3 cm
Protection Class	IP54

This device captures high density point clouds in near real-time at a rate of 300.000 points per second and has a range of up to 100 meters. It utilizes an inertial measurement unit (IMU) and Simultaneous Localization and Mapping (SLAM) algorithms to achieve a relative accuracy of up to 6 millimeters, depending on the environment which made it the ideal equipment for this project.

For the exterior and for the roofs of the buildings a DJI Mavic 3 Enterprise (Figure 2), equipped with a high-resolution imaging sensor, was deployed, enabling wide-scale coverage at various altitudes and oblique angles resulting in aerial imagery for photogrammetric processing. The technical specifications of the DJI Mavic 3 Enterprise, employed for aerial data collection, are detailed in Table 2.

Figure 2. DJI Mavic 3 Enterprise

Table 2. DJI Mavic 3 Enterprise technical specifications

Aircraft	
Weight	915 g
Max take-off weight	1050 g
Max flight speed	15 m/s (Normal Mode)
Max wind speed resistance	12 m/s
Max flight time (no wind)	45 mins
GNSS	GPS+Galileo+BeiDou+GLONASS (GLONASS is supported only when the RTK module is enabled)
Operating temperature range	-10° to 40°C
Max Pitch Angle	30° (Normal Mode) 35° (Sport Mode)
Max Angular Velocity	200°/s
Wide Camera	
Sensor	4/3 CMOS, Effective pixels: 20 MP
Lens	FOV: 84° Format Equivalent: 24 mm Aperture: f/2.8-f/11 Focus: 1 m to ∞
ISO Range	100-6400
Shutter Speed	Electronic Shutter: 8-1/8000 s Mechanical Shutter: 8-1/2000 s
Max Image Size	5280×3956
Ghimbal	
Stabilization	3-axis (tilt, roll, pan)
Mechanical Range	Tilt: -135° to 100° Roll: -45° to 45° Pan: -27° to 27°
Controllable Range	Tilt: -90° to 35° Pan: Not controllable
Max Control Speed	100°/s
Angular Vibration Range	±0.007°

To ensure proper georeferencing and alignment of data sets, ground control points were placed throughout the area of interest. The distribution of these points was influenced by existing vegetation, accessibility constraints, varying floor elevations and isolated structures.

A total of 50 ground control points were surveyed using a Trimble R10 GNSS receiver and a Trimble Geodimeter 5000 Series Total

Station in places where GPS signal was obstructed and on the facade of the buildings (Figure 3). This approach is in line with similar studies that emphasize the necessity of combining ground-based control methods with aerial and LiDAR data to ensure spatial coherence (Son et al., 2020).

Figure 3. Distribution of ground control points

The ground control points used for georeferencing the spatial data are listed in Table 3.

Table 3. Ground control points used for georeferencing

ID	X [m]	Y [m]	Z [m]
1C	397983.415	320330.852	97.22
2C	398026.357	320271.036	97.23
3C	397987.333	320325.041	86.31
4C	397999.317	320300.834	90.34
5C	398003.089	320295.676	90.41
6C	398021.967	320276.478	86.40
7C	398067.865	320391.053	97.34
8C	398074.750	320395.231	94.55
9C	398110.599	320331.028	97.19
10C	398236.541	320322.801	97.29
11C	398188.794	320388.529	97.67
12C	398208.191	320372.677	101.14
13C	398232.677	320338.422	101.15
14C	398285.683	320368.307	97.56
15C	398287.387	320387.713	99.18
16C	398262.451	320422.548	99.12
17C	398281.931	320373.321	101.06
18C	398257.741	320407.651	101.16
19C	398243.615	320427.338	97.61
20C	398202.071	320485.712	100.06
21C	398215.934	320479.656	98.90
22C	398212.722	320470.714	106.41
23C	398223.587	320455.645	106.44
24C	398240.667	320445.206	98.80
25C	398234.269	320440.692	99.97
26C	398147.486	320446.756	100.06
27C	398158.116	320431.829	106.45
28C	398168.994	320416.626	106.45

A subset of these control points was not used in the georeferencing process, instead they served as verification markers to assess the accuracy of the final merged data set. Verification points are used to provide an independent check on alignment errors and is recommended in large scale surveying projects (Salzano et al., 2024). The ground control points utilized for the verification of spatial accuracy are presented in Table 4.

Table 4. Ground control points used for verification

ID	X [m]	Y [m]	Z [m]
30V	397991.781	320319.529	95.75
31V	397997.310	320311.693	95.81
32V	398012.675	320290.222	95.75
33V	398016.155	320285.396	95.61
34V	398047.468	320286.101	95.66
35V	398094.811	320319.848	95.67
36V	398101.300	320357.350	89.28
37V	398100.105	320359.088	89.33
38V	398193.174	320382.344	90.55
39V	398195.124	320379.612	90.55
40V	398224.435	320338.345	90.62
41V	398226.432	320335.641	90.57
42V	398222.296	320352.961	101.19
43V	398218.775	320358.001	101.21
44V	398281.792	320395.517	97.59
45V	398273.270	320407.371	97.54
46V	398217.892	320476.944	97.68
47V	398238.669	320447.953	97.65
48V	398161.659	320426.547	103.75
49V	398165.165	320421.694	103.70
30V	397991.781	320319.529	95.75
31V	397997.310	320311.693	95.81
32V	398012.675	320290.222	95.75
33V	398016.155	320285.396	95.61
34V	398047.468	320286.101	95.66
35V	398094.811	320319.848	95.67
36V	398101.300	320357.350	89.28
37V	398100.105	320359.088	89.33
38V	398193.174	320382.344	90.55

Data processing consisted in converting the raw LiDAR scans into georeferenced point clouds through the manufacturer's proprietary software, which facilitates simultaneous localization and mapping (SLAM) algorithms. Initial denoising operations entailed statistical outlier detection and removal, aimed particularly at mitigating irregularities caused by reflective surfaces, shattered glass and metal debris. These operations aligned with protocols noted in earlier research, where industrial sites frequently produce erroneous reflections in laser-based recordings (Zakaria et al., 2025).

The aerial imagery was processed using Agisoft Metashape 2.0, generating an independent three-dimensional point cloud. The software automatically identified tie points through feature matching followed by a bundle adjustment procedure to optimize camera orientations and intrinsic parameters.

Georeferencing was completed by incorporating the ground control points.

The point cloud was generated using the depth maps computed for each image by stereo-

matching algorithms. The resulting point cloud was then filtered by removing redundant points, outliers and noise. The filtering was done using iterative statistical filtering and confidence-based filtering, as recommended by (Zakaria et al., 2025), to eliminate the noise derived from unstructured debris piles and partial obstructions, therefor consolidating a more homogeneous and trustworthy dataset.

After generating and filtering the LiDAR and photogrammetric point clouds, the datasets were imported into Trimble Business Center for co-registration. Tie points were first manually identified in overlapping areas to ensure rough alignment, followed by refinement using the iterative closest point algorithm, as applied in similar complex survey environments (Abreu et al., 2023).To quantify the quality of the merged data, a series of verification points (Table 4), distinct from the control points used for georeferencing (Table 3), were surveyed on-site using the Total Station and then compared to their corresponding positions in the unified point cloud. Figure 4 illustrates the verification points used to assess the accuracy of the merged dataset.

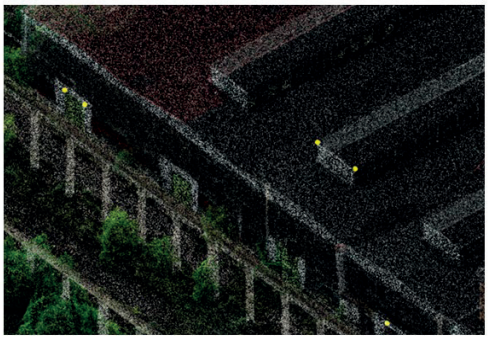

Figure 4. Verification points

The root means square errors and the probable error along the X, Y and Z axes were computed to characterize horizontal and vertical deviations as shown in (Table 5).

Once the point clouds had been successfully fused, they served as the foundation for constructing a three-dimensional model of the industrial complex. In the initial stage of this modeling process, three horizontal cross-sections were extracted from the point cloud at the ground level, as well as the first and second floors (Figure 5). These cross-sections provided the reference data necessary to generate accurate floor plans for each building within the complex. Subsequently, vertical sections were derived along each principal building axis (Figure 6), and the combined use of horizontal and vertical cross-sections enabled precise modeling of all structural elements.

Each modeled component was then classified according to its constituent material (e.g., concrete, metal, wood, or glass).

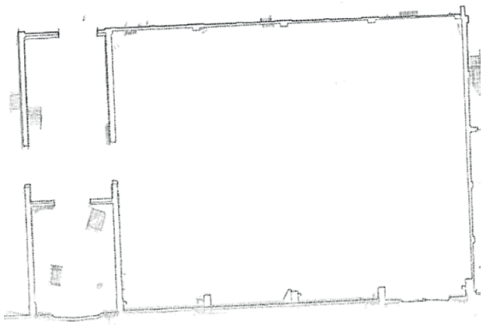

Figure 5. Horizontal section of the point cloud

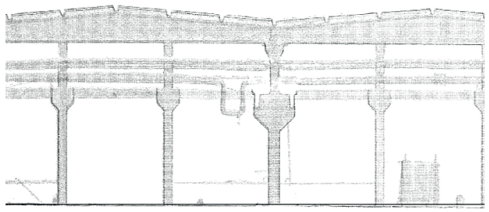

Figure 6. Vertical section of the point cloud

Studies focusing on point cloud–to–CAD workflows in complex industrial environments highlight the recurring challenges posed by irregular geometries, occlusions, and noise (Abreu et al., 2023).

Table 5. Precision estimate

Point code	Field survey			Points in the point cloud			Δ		
	X1 [m]	Y1 [m]	Z1 [m]	X2 [m]	Y2 [m]	Z2 [m]	ΔX [m]	ΔY [m]	ΔZ [m]
30V	397991.781	320319.529	95.75	397991.708	320319.461	95.74	0.073	0.068	0.01
31V	397997.310	320311.693	95.81	397997.304	320311.661	95.72	0.006	0.032	0.09
32V	398012.675	320290.222	95.75	398012.658	320290.257	95.69	0.017	-0.034	0.06
33V	398016.155	320285.396	95.61	398016.112	320285.441	95.68	0.043	-0.044	-0.07
34V	398047.468	320286.101	95.66	398047.411	320286.063	95.64	0.057	0.038	0.02
35V	398094.811	320319.848	95.67	398094.886	320319.817	95.63	-0.075	0.031	0.04
36V	398101.300	320357.350	89.28	398101.321	320357.351	89.30	-0.020	-0.001	-0.02
37V	398100.105	320359.088	89.33	398100.188	320359.097	89.40	-0.083	-0.008	-0.06
38V	398193.174	320382.344	90.55	398193.161	320382.32	90.54	0.013	0.024	0.01
39V	398195.124	320379.612	90.55	398195.093	320379.634	90.54	0.031	-0.021	0.01
40V	398224.435	320338.345	90.62	398224.419	320338.328	90.58	0.016	0.017	0.03
41V	398226.432	320335.641	90.57	398226.402	320335.637	90.55	0.030	0.005	0.02
42V	398222.296	320352.961	101.19	398222.333	320353.021	101.19	-0.036	-0.059	-0.01
43V	398218.775	320358.001	101.21	398218.838	320358.050	101.20	-0.062	-0.048	0.01
44V	398281.792	320395.517	97.59	398281.738	320395.611	97.54	0.054	-0.093	0.04
45V	398273.270	320407.371	97.54	398273.325	320407.358	97.58	-0.054	0.013	-0.03
46V	398217.892	320476.944	97.68	398217.817	320476.938	97.64	0.075	0.006	0.03
47V	398238.669	320447.953	97.65	398238.598	320447.893	97.64	0.071	0.060	0.01
48V	398161.659	320426.547	103.75	398161.647	320426.533	103.76	0.012	0.015	-0.01
49V	398165.165	320421.694	103.70	398165.159	320421.689	103.77	0.006	0.005	-0.06
Root mean square Error: $e_m=\pm\frac{m}{\sqrt{n}}$, where $m=\pm\sqrt{\frac{[vv]}{n-1}}$							**±0.048**	**±0.039**	**±0.039**
Probable error: $e_p=\pm\frac{2}{3}e_m$							**±0.032**	**±0.026**	**±0.026**

In the Dolj Chim project, structural complexity was addressed through the use of repetitive, prefabricated elements - particularly standardized concrete beams - a strategy aligned with approaches used in projects involving repetitive architectural components (Abreu et al., 2023). The merged point cloud facilitated the extraction and visualization of key structural elements within the industrial complex. As shown in Figure 7, the resulting 3D model accurately represents the spatial and architectural configuration of the site, forming a reliable basis for further spatial analyses, documentation, and integration into planning or monitoring processes.

To assess surface material accumulation, Figure 8 illustrates the debris volume derived from the processed point cloud. This sheet displays the spatial distribution and elevation variation of debris, enabling quantitative evaluation necessary for planning site clearance, estimating transport needs, and assessing environmental impact.

Figure 7. 3D elements of the industrial complex

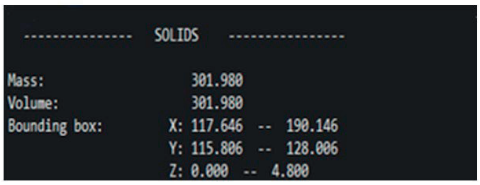

Figure 8. Debris volume sheet

Following the completion of the full 3D model (Figure 10), it was possible to estimate the total volume of debris projected from demolition

activities. Calculations were conducted separately for each material class. The results were compiled into dedicated volume sheets that specify debris quantities by material type, allowing for more accurate planning and resource allocation. The final material-specific volume estimates are presented in Figure 9.

For more complex structural components, such as reinforced concrete, it was necessary to estimate the internal steel content. To this end, standardized material ratios were applied, and the corresponding values used for these calculations are presented in Table 6.

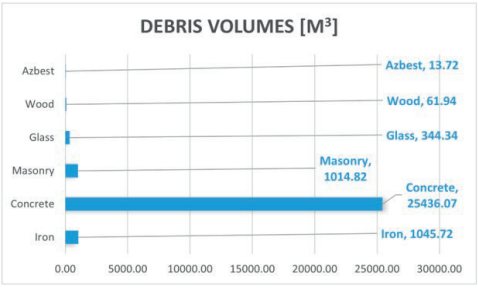

Figure 9. Bar chart representing debris values

Table 6. Amount of iron in complex structures

Element	Iron [kg/m³]
Foundation structure	40
Structural framework	100
Concrete wall structure	80
Floor slab	80
Roof slab	60

The final stage of the workflow involved the preparation of a comprehensive bill of quantities, detailing the demolition costs for each individual structure alongside associated expenses for logistics, environmental remediation, and labor. This cost assessment highlights the critical value of integrating detailed 3D modeling with economic and environmental parameters - an approach that is increasingly acknowledged as best practice in modern industrial demolition planning.

RESULTS AND DISCUSSIONS

The circular economy and the recycling of construction materials are essential strategies for reducing the negative impact on the environment. In this context, accurately determining the value of construction waste resulting from demolition is a critical element for the conservation of natural resources and the development of a more sustainable and economically efficient construction sector (Oliveira, Schreiber & Jahno, 2024).

The final integrated point cloud provided a comprehensive depiction of the Dolj Chim industrial complex, encompassing both interior and exterior elements in a single, unified coordinate system. The RMSE and probable error values underscored the high fidelity of the merged dataset and align with benchmarks reported in comparable industrial scanning endeavours (Gibson & Alderson, 2019; Zhan et al., 2020).

The final dataset achieved high georeferencing accuracy, with a mean square error (MSE) of ±0.048 meters in the X-axis, ±0.039 meters in the Y-axis, and ±0.039 meters in the Z-axis. The probable error values were ±0.032 meters in the X-axis, ±0.026 meters in the Y-axis, and ±0.026 meters in the Z-axis (Table 5). These values indicate a high level of precision, ensuring that the resulting point cloud was reliable for demolition volume estimation.

Notably, the LiDAR system achieved superior results in capturing enclosed spaces devoid of strong ambient illumination, whereas the UAS-derived photogrammetry excelled in mapping extensive exterior surfaces and rooftops. These findings reaffirm established conclusions from parallel studies, which highlight the complementary nature of LiDAR and photogrammetry in scenarios that demand both detailed internal scans and large-scale external mapping (Zakaria et al., 2025; Son et al., 2020).

The differences between the LiDAR and UAS-based point clouds were evident due to the nature of the data collection methods. The UAS-generated point cloud, being a product of photogrammetric processing, exhibited a more uniform structure resembling a "sheet" draped over the buildings. In contrast, the LiDAR-derived dataset was denser and contained more irregularities, capturing finer details of the structures. Although these datasets did not align perfectly due to their inherent differences, the integration of control points allowed for an acceptable level of matching that met project requirements.

The efficiency gains achieved through this integrated approach were significant. The entire data collection phase was completed within

three days, a fraction of the time required for traditional methods, which could have taken weeks. Traditional surveying would have been especially challenging in this case due to the lack of sufficient lighting inside the buildings, making it nearly impossible to obtain detailed measurements without advanced scanning technology. Additionally, the availability of drone imagery and LiDAR data significantly reduced human error, as surveyors had comprehensive datasets to reference instead of relying solely on manually collected points and field notes.

In conjunction with precise 3D reconstruction, attention was directed toward the potential integration of Building Information Modeling (BIM) in demolition planning. Although BIM has historically been employed for new construction, its application in demolition contexts (Salzano et al., 2024) has grown in recent years owing to increased awareness of sustainability and resource management issues (Nikmehr et al., 2021). The detailed as-built data generated in this study can serve as a basis for a retrospective BIM, thus offering significant advantages in managing the dismantling of complex industrial structures. Empirical studies suggest that a robust BIM framework can reduce construction and demolition waste by optimizing the quantity and reusability of extracted materials (Nikmehr et al., 2021). While the Dolj Chim complex predates widespread BIM adoption, the dataset assembled here can streamline sustainable demolition procedures by enabling precise volume calculations, safety assessments, and resource allocation (Sestras et al., 2025).

Furthermore, a comparative analysis of the Dolj Chim survey with similar multi-sensor projects revealed numerous shared benefits and recurring obstacles. One frequently encountered challenge in industrial environments is the presence of heavy clutter or debris, which can generate considerable levels of noise in raw point clouds (Zakaria et al., 2025). The Dolj Chim dataset exemplified this issue but benefited from repeated structural designs and standard prefabricated elements, thereby alleviating some of the modeling difficulties. This finding is consistent with research indicating that templated modeling and semi-automated segmentation can reduce the manual labor required for point cloud processing in repetitive architectural environments (Abreu et al., 2023; Gibson & Alderson, 2019). Nonetheless, further work is required to optimize these processing pipelines, especially when such workflows must contend with expansive, congested, or partially collapsed structures.

One of the key improvements noted from this project was the realization that excessive data collection could be a challenge. In this case, the slow pace of LiDAR scanning resulted in a very large dataset, which increased processing time. To optimize future projects, a higher walking speed was adopted in subsequent surveys, reducing unnecessary data density while maintaining accuracy. Additionally, future projects included a greater number of control points inside buildings where conditions allowed, further improving georeferencing quality.

Overall, this study demonstrated that integrating LiDAR and UAS-based photogrammetry provides a robust and efficient method for industrial demolition planning. The approach is adaptable to various environments, though urban applications may require special permissions for UAS flights.

CONCLUSIONS

The integrated LiDAR and photogrammetric methodology employed in this study proved highly effective for generating an accurate and comprehensive 3D model of the Dolj Chim industrial complex (Figure 10).

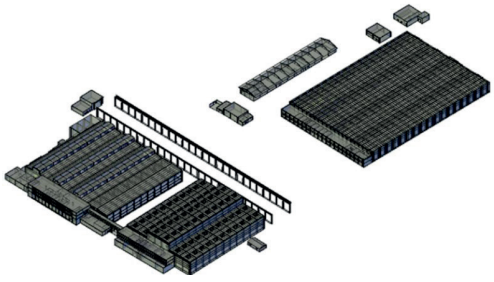

Figure 10. 3D model of Dolj Chim industrial complex

By leveraging the respective strengths of high-density interior scanning and wide-area exterior imaging, this approach yielded precise data for volume estimation, despite the presence of degraded, cluttered, and poorly illuminated

structures. The resultant root means square errors aligned well with benchmarks reported in comparable industrial surveys, thereby confirming that a multi-sensor data fusion framework is vital in contexts demanding a thorough understanding of both internal and external site conditions (Son et al., 2020).

In addition, this study reinforces the growing importance of integrating as-built 3D data into BIM-driven workflows. Although the Dolj Chim facility was not originally modeled in BIM, the accurate digital data obtained here can facilitate subsequent retrospective modeling, an approach that promises to improve demolition planning and waste management (Nikmehr et al. 2021). Future efforts should examine ways to refine data processing routines, particularly with respect to advanced feature recognition and template-based modeling, as these techniques could further accelerate the extraction of 2D and 3D deliverables (Abreu et al. 2023). Enhanced scanning speeds, improved dynamic SLAM capabilities, and expanded use of indoor GCPs stand as promising directions for achieving still greater accuracy and operational efficiency.

The methodological insights gained through this project appear highly transferable to similar industrial or urban settings, with the principal constraint being regulatory limitations on drone operation and on-site safety considerations. Consequently, this study contributes practical and theoretical knowledge that can inform subsequent surveys and research. By bridging multiple data sources and adopting rigorous registration processes, scholars and practitioners alike can develop robust, data-rich models that foster safer, more sustainable, and more cost-effective demolition projects.

ACKNOWLEDGEMENTS

This research work was carried out and financed with the support of GAUSS S.R.L. The authors wish to acknowledge the invaluable assistance of the site management team and all colleagues who contributed to the data collection and processing stages.

REFERENCES

Abreu, N., Pinto, A., Matos, A., & Pires, M. (2023). Procedural point cloud modelling in scan-to-BIM and scan-vs-BIM applications: A review. *ISPRS International Journal of Geo-Information, 12*(7), 260. https://doi.org/10.3390/ijgi12070260

DJI (2022). *Mavic 3 Enterprise Series - Product Specifications*. https://www.dji.com

GeoSLAM. (2022). *Zeb Horizon RT LiDAR Scanner - Technical Datasheet*. https://geoslam.com

Matsimbe, J., Mdolo, W., Kapachika, C., Musonda, I., & Dinka, M. (2022). Comparative utilization of drone technology vs. traditional methods in open pit stockpile volumetric computation: A case of Njuli quarry, Malawi. *Frontiers in Built Environment, 8*, 1037487. https://doi.org/10.3389/fbuil.2022.1037487

Nikmehr, B., Hosseini, M. R., Wang, J., Chileshe, N., & Rameezdeen, R. (2021). BIM-based tools for managing construction and demolition waste (CDW): A scoping review. *Sustainability, 13*(15), 8427. https://doi.org/10.3390/su13158427

Oliveira, J. de, Schreiber, D., & Jahno, V. D. (2024). Circular economy and buildings as material banks in mitigation of environmental impacts from construction and demolition waste. *Sustainability, 16*(12), 5022. https://doi.org/10.3390/su16125022

Son, S. W., Kim, D. W., Sung, W. G., & Yu, J. J. (2020). Integrating UAV and TLS approaches for environmental management: A case study of a waste stockpile area. *Remote Sensing, 12*(10), 1615. https://doi.org/10.3390/rs12101615

Trimble (2019). *Trimble Geodimeter 5000 Series - Technical Specifications*. https://www.trimble.com

Trimble (2021). *Trimble R10 GNSS Receiver - User Guide*. https://www.trimble.com

Zakaria, M. H., Fawzy, H., El-Beshbeshy, M., & Farhan, M. (2025). A comparative study of terrestrial laser scanning and photogrammetry: Accuracy and applications. *Civil Engineering Journal, 11*(3), 1196–1216. https://doi.org/10.28991/CEJ-2025-011-03-021

Nikmehr, B., Hosseini, M. R., Wang, J., Chileshe, N., & Rameezdeen, R. (2021). BIM-Based Tools for Managing Construction and Demolition Waste (CDW): A Scoping Review. *Sustainability, 13*(15), 8427. https://doi.org/10.3390/su13158427

Salzano, A., Cascone, S., Zitiello, E. P., & Nicolella, M. (2024). Construction Safety and Efficiency: Integrating Building Information Modeling into Risk Management and Project Execution. *Sustainability, 16 (10), 4094.* https://doi.org/10.3390/su16104094

Sestras, P., Badea, G., Badea, A. C., Salagean, T., Roșca, S., Kader, S., & Remondino, F. (2025). Land surveying with UAV photogrammetry and LiDAR for optimal building planning. *Automation in Construction, 173, 106092.* https://doi.org/10.1016/j.autcon.2025.106092